


Transition metal atom adsorption on the titanium carbide MXene: Trends across the periodic table for the bare and O-terminated surfaces

Henrique Rocha , José D. Gouveia *, and José R. B. Gomes †

CICECO – Aveiro Institute of Materials, Department of Chemistry, University of Aveiro, Campus Universitário de Santiago, 3810-193 Aveiro, Portugal

 (Received 9 June 2022; revised 19 August 2022; accepted 16 September 2022; published 14 October 2022)

MXenes are a family of two-dimensional materials of great interest due to their unique properties, e.g., adjustability based on changes in their composition, structure, and surface functionality, which grant MXenes a variety of applications. One way of changing the catalytic effect of MXenes consists of adsorbing isolated metallic elements, such as transition metals (TMs), onto their surface, leading to the formation of single-atom catalysts. Herewith, the adsorption behavior of 31 TMs on the surface of two titanium carbide MXenes, viz. Ti_2C and Ti_2CO_2 , is analyzed by means of density-functional theory (DFT) calculations. We find that the oxygen surface termination causes most of the TM atoms to adsorb on a hollow site above a carbon atom, whereas on bare Ti_2C , the adsorption preference follows a pattern related to groups of the periodic table. The interaction between the TM atoms and the surface of both Ti_2C and Ti_2CO_2 is strong, as demonstrated by the calculated adsorption energies, which range between about -1 and -9 eV on either surface. Upon adsorption on Ti_2CO_2 , electrons are transferred from the adatom to the MXene surface, whereas on Ti_2C , the only TM atoms for which this happens are the ones in group 3 of the periodic table. All the other transition metal atoms become negatively charged after adsorption on Ti_2C . On the oxygen-covered MXene, stronger adsorptions are accompanied by higher charge transfers. The energy barriers for TM adatom diffusion on Ti_2C are very small, meaning that the adatoms can move rather freely along it. On Ti_2CO_2 , however, higher diffusion barriers were found, many being above 1 eV, which suggests that the oxygen termination layer blocks the diffusion. On both surfaces, the highest diffusion barriers were found to correspond to the TM elements which adsorb most strongly.

DOI: [10.1103/PhysRevMaterials.6.105801](https://doi.org/10.1103/PhysRevMaterials.6.105801)

I. INTRODUCTION

Since the seminal studies developed by Geim and Novoselov concerning the exfoliation of graphene [1], the interest in two-dimensional (2D) materials by the scientific community soared, leading not only to the intensive study of existing 2D materials, but also to the discovery of new materials, whose captivating properties have prompted their application in diverse areas. MXenes are among these new materials and typically consist of 2D carbides, nitrides, or carbonitrides of a particular transition metal. The first MXene, $Ti_3C_2T_x$, was discovered in 2011 [2] and, so far, it is the one that has received the most attention. Since then, more than 30 distinct MXenes have been experimentally synthesized and the structures of many others have been computationally predicted [3].

MXenes have unique properties, which can be adjusted by changing their composition, functionalizing their surface, and changing their structure/morphology [4–14]. Because of this, MXenes are a very versatile family of materials, displaying great utility in many areas [15–28]. In addition to their use in energy storage [4,16–19], biomedical applications [20], sensors [26–28], and many other fields, MXenes play an im-

portant role as catalysts, mainly due to their large surface area, which implies more active sites. In fact, MXenes have already been used as catalysts in the hydrogen evolution reaction [29], nitrogen reduction reaction [30], CO_2 functionalization [31], and CO_2 reduction [32]. Relevant computational studies have also already been developed for a detailed understanding of the catalytic mechanisms [22,25,33–35]. These reactions can be carried out with the formation of single-atom catalysts (SACs), which consist of catalysts in which an active metal species is present in the form of isolated atoms bonded to another metallic species (in this case, to the surface of the MXene) [23,31,36,37]. This strategy exhibits great potential since it can increase the stability, activity, and selectivity of MXenes [24]. The large surface area and the possibility of manipulating the terminations of these materials facilitate the adsorption and stabilization of the isolated atoms [38] which, once adsorbed, redistribute the electronic structure of the MXenes, hence altering their properties. This approach benefits greatly from the use of transition metals as the isolated atoms to be adsorbed. This is due to the catalytic performance of metals being often improved if a mixture of metals is used, instead of a single-elemental catalyst [39]. Since MXenes are essentially made up of transition metals, the adsorption of atoms of metallic elements different from those existing in the parent MXene can drastically improve the catalytic effect of these materials. The formation of SACs on MXene surfaces has already been considered by Illas and co-workers [40,41],

*gouveia@ua.pt

†jrgomes@ua.pt

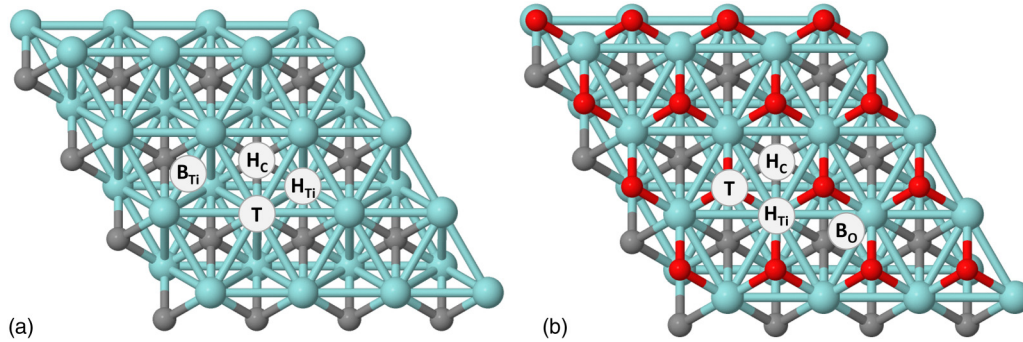


FIG. 1. Top view of the $p(4 \times 4)$ supercells employed to model the (a) Ti_2C and (b) Ti_2CO_2 MXene surfaces. Titanium atoms are shown as teal blue spheres, while the carbon atoms are shown as gray spheres. Red spheres represent the oxygen atoms in Ti_2CO_2 . Labels refer to the four relevant high-symmetry sites on each surface: bridge (between titanium atoms, B_{Ti} , and between oxygen atoms, B_{O}), top (T), hollow titanium (H_{Ti}), and hollow carbon (H_{C}).

but only the first-row transition metals were covered in these studies.

The $\text{Ti}_3\text{C}_2\text{T}_X$ MXene has been the focus of most studies devoted to this family of materials, which implies a deep knowledge of this material and, consequently, the existence of useful reference values for the treatment of the obtained results. That being said, the present study focuses on similar but less complex MXenes with stoichiometry Ti_2CT_X , both without surface termination and with oxygen termination. The oxygen coverage was chosen, since studies reveal better thermodynamic stability and better conductivity in MXenes with this termination [11].

This study aims to determine the adsorption behavior of transition metal atoms on the surface of Ti_2C and Ti_2CO_2 , by employing computer modeling techniques, based on the density-functional theory. In the following, we describe the computational method, followed by a presentation of the results, focusing on structural and energetic data, and a summary of the conclusions. The Supplemental Material [42] includes additional tables and figures with energies, distances, and additional values and correlations that complement the discussion in the main text.

II. MXene MODELS AND COMPUTATIONAL DETAILS

This study relies on first-principles calculations based on density-functional theory (DFT), using the Vienna *Ab initio* Simulation Package (VASP) [43–46]. The calculations were performed within the generalized gradient approximation to the many-body exchange-correlation functional, using the functional introduced by Perdew, Burke, and Ernzerhof (PBE) [47], with the contribution of dispersion terms approximated through the DFT-D3 method, proposed by Grimme [48,49]. This exchange-correlation setup is commonly used to describe adsorption phenomena on MXenes, so it was chosen here to allow comparison of the present results with those of previous works, both ours [25–27,33,34] and from other authors [40,41]. Moreover, PBE-D3–level DFT results [50] have been confirmed experimentally [51] for the specific case of CO_2 interaction with MXene carbides.

The representative models of the MXene surfaces under study (Fig. 1) consist of periodic $p(4 \times 4)$ supercells, with dimensions $a = b = 12.16 \text{ \AA}$ and $c = 21.21 \text{ \AA}$, for bare Ti_2C ,

and $a = b = 12.14 \text{ \AA}$ and $c = 24.09 \text{ \AA}$, for the O-terminated MXene. The lengths of a and b were optimized, while the length of the supercell in the direction perpendicular to the MXene surface plane guarantees the presence of at least $\sim 13 \text{ \AA}$ of vacuum between the periodic replicas of the system, even after the adsorption of a transition metal atom.

The valence electron density was expanded on a plane-wave basis set with an energy cutoff of 415 eV. The effect of the remaining electrons was considered using the projector augmented-wave method [52]. The valence electron configuration of each metallic element used in this study is available in Table S1 of the Supplemental Material. The convergence criterion for the self-consistent field energies was defined as 10^{-5} eV and structures were considered relaxed when the forces acting on all atoms were lower than 0.01 eV/\AA . To perform the necessary numerical integrations in the reciprocal space, the Brillouin zone was sampled using a Monkhorst-Pack $3 \times 3 \times 1$ grid of automatically generated k points, centered on the gamma point [53].

Spin polarization was considered in all calculations and only produced significant differences in the energies or positions obtained for Nb and La adsorptions on the Ti_2C surface and for Mn, Fe, and Co on the Ti_2CO_2 surface.

In order to investigate the behavior of each transition metal near the MXene surface, the atom of the metal in question was initially positioned close to each of the four high-symmetry locations (Fig. 1) on each MXene. The metal atom was not positioned exactly above these locations, as the high symmetry of this configuration could force the atom to be adsorbed on that site, even if that position was unstable.

For the most stable position of each metal, on either MXene, the adsorption energy (E_{ads}) and the electronic charge transfer between the MXene surface and the adsorbed atom were calculated. Here, the adsorption energy (E_{ads}) is defined as

$$E_{\text{ads}} = E_{\text{MXene+TM}} - (E_{\text{MXene}} + E_{\text{TM}}), \quad (1)$$

where $E_{\text{MXene+TM}}$, E_{MXene} , and E_{TM} stand for the total energies of a supercell containing the MXene with the adsorbed transition metal atom, the clean MXene surface, and the isolated transition metal atom, respectively. The charge transfer is the difference between the number of explicitly treated electrons from the TM atom before and after its adsorption on

TABLE I. Preferred adsorption site for a transition metal atom on Ti_2C . Labeling of adsorption sites is the same as in Fig. 1(a).

Sc	Ti	V	Cr	Mn	Fe	Co	Ni	Cu	Zn
B_{Ti}	B_{Ti}	B_{Ti}	H_{C}	H_{C}	H_{C}	H_{C}	H_{C}	H_{Ti}	H_{Ti}
Y	Zr	Nb	Mo	Tc	Ru	Rh	Pd	Ag	Cd
B_{Ti}	B_{Ti}	H_{C}	H_{C}	H_{C}	H_{C}	H_{C}	H_{C}	H_{Ti}	H_{Ti}
La/Lu	Hf	Ta	W	Re	Os	Ir	Pt	Au	Hg
B_{Ti}	B_{Ti}	B_{Ti}	H_{C}	H_{C}	H_{C}	H_{C}	H_{C}	H_{Ti}	H_{Ti}

the MXene. Thus, positive or negative charge-transfer values represent the transference of electrons from the TM atom to the MXene surface and vice versa, respectively. The number of electrons present on the adsorbed TM atom was estimated through a Bader analysis of the electron density [54].

III. RESULTS

The behavior of transition metal atoms when adsorbed onto the surface of Ti_2C and Ti_2CO_2 was analyzed by calculating the adsorption site, adsorption energy, and charge transferred between the adsorbed atom and the MXene surface.

A. Structural data

Tables I and II contain the results obtained for the preferred adsorption site on Ti_2C and Ti_2CO_2 , respectively.

Regarding Ti_2C , i.e., the thinnest titanium carbide MXene with no surface termination, by analyzing Table I, one can observe a correlation between the filling of the d subshell of a transition metal atom and its preferred adsorption position. Early transition metals (groups 3–5, with 1–4 d electrons) tend to be adsorbed in a bridge site. Niobium (Nb) is the only metal from group 5 that prefers to be adsorbed on a hollow carbon site, with this adsorption site being nearly as stable as the bridge between titanium atoms, which follows the trend mentioned (the difference in energy between adsorption on either site is only 0.05 eV). Late transition metals (groups 11 and 12, with a full d shell) tend to be adsorbed in a hollow titanium site. All the other transition metals (groups 6–10) tend to adsorb in a hollow carbon site.

On Ti_2CO_2 , the same pattern is not observed. Due to the presence of oxygen atoms, nearly all transition metal atoms show greater stability when adsorbed on a hollow carbon site [see Fig. 1(b)], where they are able to bond with 3 titanium atoms and 3 oxygen atoms. A few exceptions were observed. For instance, osmium (Os), iridium (Ir), and platinum (Pt) show higher stability when adsorbed on a bridge site, palladium (Pd) prefers a hollow titanium site, and gold (Au) shows greater stability when adsorbed on a top position, bonded

TABLE II. Preferred adsorption site for a transition metal atom on Ti_2CO_2 . Labeling of adsorption sites is the same as in Fig. 1(b).

Sc	Ti	V	Cr	Mn	Fe	Co	Ni	Cu	Zn
H_{C}	H_{C}	H_{C}	H_{C}	H_{C}	H_{C}	H_{C}	H_{C}	H_{C}	H_{C}
Y	Zr	Nb	Mo	Tc	Ru	Rh	Pd	Ag	Cd
H_{C}	H_{C}	H_{C}	H_{C}	H_{C}	H_{C}	H_{C}	H_{Ti}	H_{C}	H_{C}
La/Lu	Hf	Ta	W	Re	Os	Ir	Pt	Au	Hg
H_{C}	H_{C}	H_{C}	H_{C}	H_{C}	B_{O}	B_{O}	B_{O}	T	H_{C}

to the oxygen atom with a bond order of 0.89 (determined using the DDEC6 method described in Ref. [55]). In accordance with this, other studies have also found higher structural stability when a single gold atom is primarily bonded to an oxygen atom, rather than to a transition metal atom [56,57]. All adsorption sites found here coincide with the ones found in Refs. [40,41] for the first-row transition metals, apart from V adsorption on Ti_2C , which was predicted to occur on an H_{C} site. One possible explanation is that, although the authors of Refs. [40,41] employed a very similar methodology, they considered a smaller, 3×3 MXene supercell and some computational parameters (e.g., number of k points or number of electrons treated explicitly) differ from the ones used in this work.

The distances between the adsorbed transition metal atom and the nearest titanium layer as well as the carbon layer of both MXenes are shown in Fig. 2. Individual values are shown in Tables S2 and S3 of the Supplemental Material, and a comparison between distances involving La (empty $4f$ subshell) and Lu (fully occupied $4f$ subshell) is displayed in Fig. S1 in the Supplemental Material. The fact that the same TM atoms are adsorbed on different sites on each MXene makes for a difficult comparison of adatom-MXene surface distances between the two supports. However, on Ti_2C , these distances initially decrease along each period of the periodic table, reaching a minimum on group 8, and increasing from thereon forward. This behavior is less evident on Ti_2CO_2 . This leads to transition metal atoms of groups 3 to 6 displaying a longer adatom-MXene distance in Ti_2C than in Ti_2CO_2 . There is also an increase in the adatom- Ti_2C distance when increasing the period number, except for TM atoms adsorbed on the hollow titanium position (and palladium) or when the adsorption site of the TM atoms of the same group does not match (group 5). It was found that the average distance between the adatom and these layers was lower on Ti_2C than on Ti_2CO_2 . This is a result of the presence of oxygen atoms in the surface of Ti_2CO_2 . The average distances between a TM atom adsorbed on Ti_2C and its carbon layer and nearest titanium layer are 1.41 and 0.87 Å, respectively, while in the case of Ti_2CO_2 , the corresponding distances are 1.45 and 0.92 Å, respectively.

On Ti_2CO_2 , the atoms of the transition metals of group 12 away from the periodic table (Zn, Cd, and Hg) were adsorbed further from the MXene surface than the rest of the metal atoms, hence establishing weaker bonds. The sum of bond orders between each of these metal atoms and the Ti_2CO_2 surface are 0.31, 0.35, and 0.25, respectively. As we will see, atoms of these elements adsorb very weakly on Ti_2CO_2 and trade nearly no charge with the surface. However, the same behavior is not observed for Ti_2C , because the undercoordinated Ti atoms lead to a much more chemically active surface termination.

B. Energetic data

The adsorption energies of an atom of each transition metal on the Ti_2C and Ti_2CO_2 MXenes are displayed in Fig. 3. The values used to build the plots are shown in Tables S4 and S5 of the Supplemental Material.

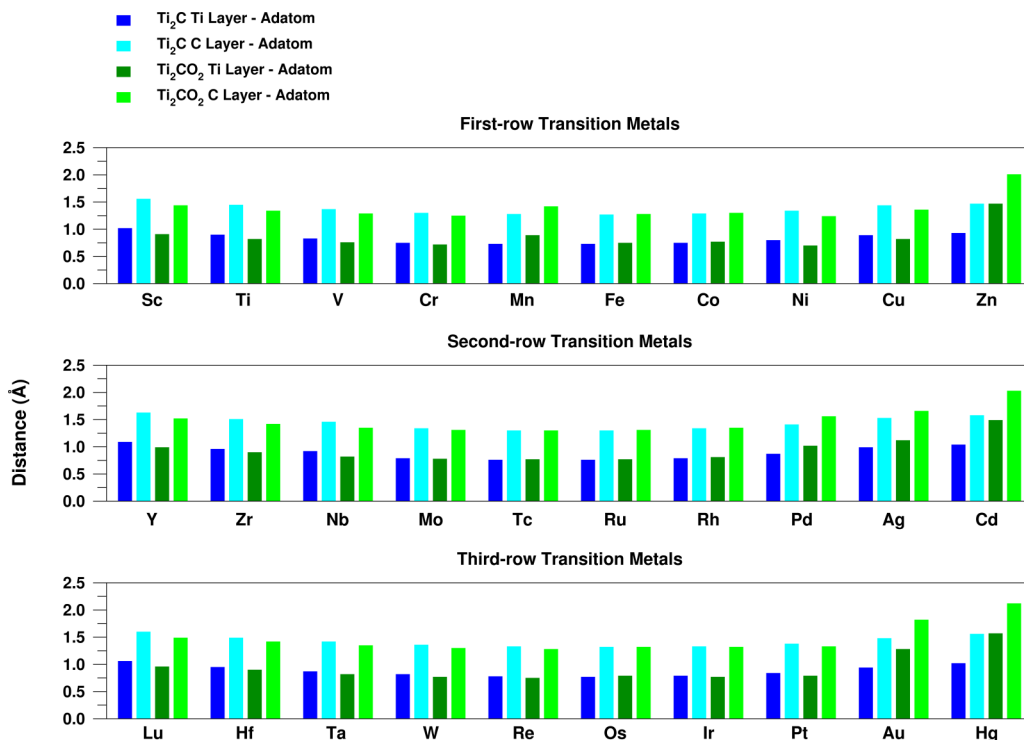


FIG. 2. Distance (in Å) between adsorbed transition metal atoms and the titanium and carbon layers closest to the adatom on Ti₂C and Ti₂CO₂.

On Ti₂C, i.e., in the absence of surface termination, the first-row TMs display an adsorption energy profile shaped like a camel hump (see left side of Fig. 3), as observed in previous studies [40]. This behavior is somewhat maintained for the second-row TMs, in which the camel hump is less pronounced but present regardless. For third-row TMs, this shape

is no longer evident. The lutetium (Lu) adsorption energy is in place with the remaining third-row TMs, while the E_{ads} of lanthanum (La) is not. This is due to different electronic occupations of the 4*f* orbitals, i.e., La has no *f* electrons, while Lu has a completely full *f* subshell, like the remaining third-row TMs.

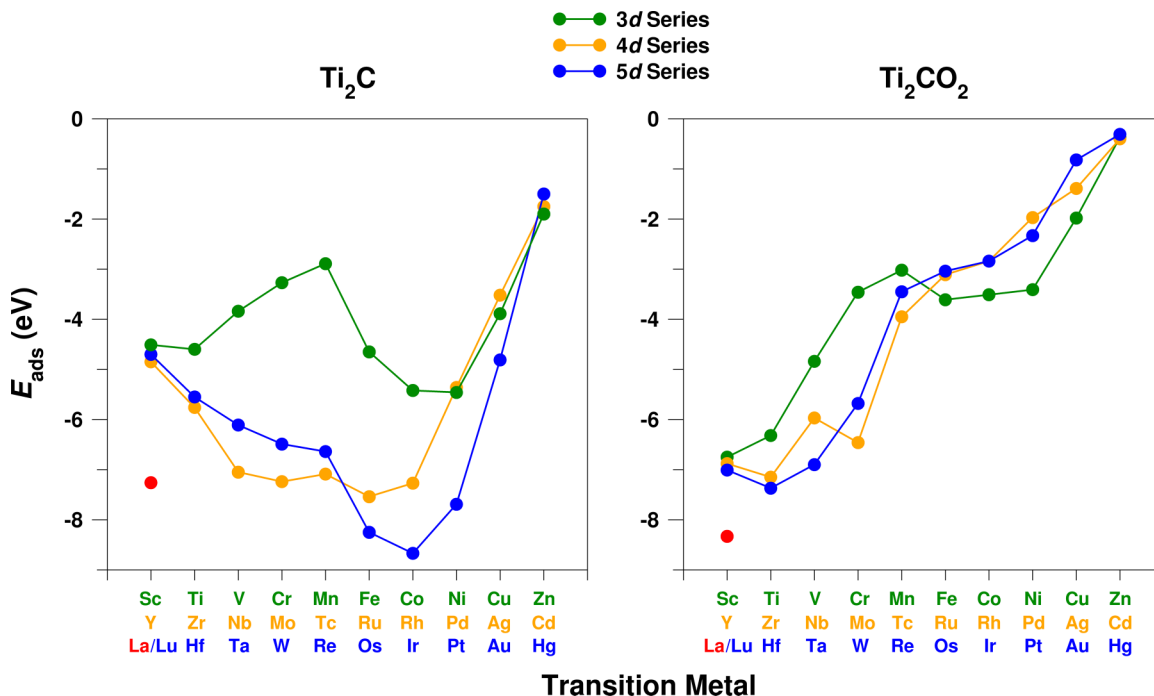


FIG. 3. Adsorption energy (in eV) of transition metals on Ti₂C (left) and Ti₂CO₂ (right).

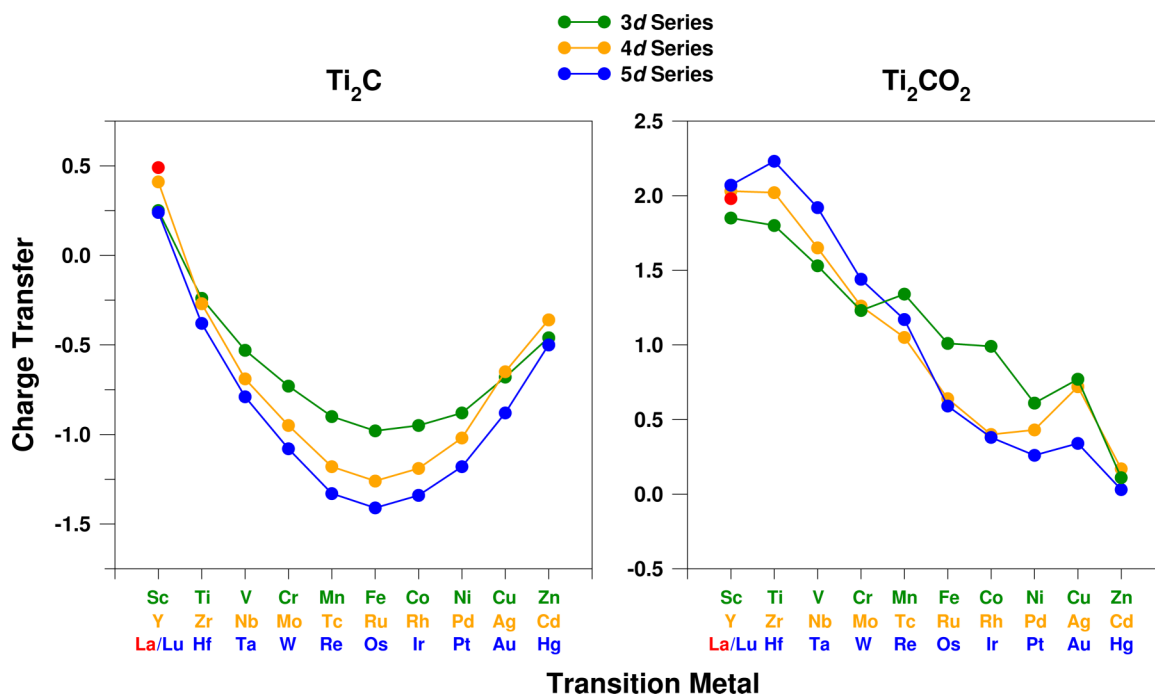


FIG. 4. Charge transfer (in units of charge of an electron) of transition metals on Ti_2C (left) and Ti_2CO_2 (right). A positive charge transfer implies that the electrons are transferred from the adatom to the MXene surface, while a negative charge transfer implies the electron transference happens in the opposite way. Note the different scales on the vertical axes of both plots. Numerical values are provided in Tables S6 and S7.

On the Ti_2CO_2 MXene, there is a more uniform behavior between transition metals of different periods (see right side of Fig. 3), where molybdenum (Mo) is the only metal that seems slightly out of place, besides lanthanum, which does not follow the trends well for the reason mentioned above. The E_{ads} values are of the same order of magnitude as the ones found for Ti_2C , but there is a predominant increase in E_{ads} (decrease of adsorption strength) along each row of the periodic table, unlike what is seen on Ti_2C .

On both MXenes, on the early transition metals, there is a clear tendency for the adsorption of the 3d series TM atoms to be weaker than those of the other two series. However, on late transition metals, the E_{ads} are very similar between TM series. In fact, on Ti_2CO_2 , on late TMs, the tendency is for the adsorption energies of the 3d series TM atoms to be more negative than those of the other two series.

Other studies of transition metal atom adsorption on MXenes display remarkably similar results as the ones presented here, despite the slight differences in methodology [40,41]. This can be realized by visually comparing our plots relative to first-row transition metal adsorption on Ti_2C and Ti_2CO_2 (green lines in Fig. 3) with Fig. 2 of Ref. [40] and Fig. 2 of Ref. [41], respectively. Concerning Ti_2C , both our plot and the one in Ref. [40] show that the adsorption energies lie between -5 eV (for Ni) and -2 eV (for Zn), with a local extremum occurring for Mn adsorption, around -3 eV. In the case of Ti_2CO_2 , our results are visually identical to the ones from Ref. [41]. Both plots indicate that the adsorption becomes weaker as we move along the period of the periodic table, and that the strongest metal adsorption occurs for Sc, with an E_{ads} of almost -7 eV, while the weakest one occurs for Zn.

As for the charge transfer upon adsorption of a TM atom on Ti_2C (see left side of Fig. 4), it is possible to observe that for each row of TMs, atoms of the elements of group 8 (Fe, Ru, and Os) transfer the most electrons from the Ti_2C surface to themselves. On this MXene, only the elements of group 3 (Sc, Y, La, and Lu) have a positive charge transfer, meaning the electrons are transferred from the metal atom to the Ti_2C surface. On Ti_2CO_2 , the charge-transfer values are all positive (see right side of Fig. 4), i.e., all adatoms become positively charged, due to the electronegativity of the oxygen atoms. The charge-transfer values also decrease along each period of the periodic table, as a result of the gradual filling of the d orbitals.

On both surfaces studied here, one finds reasonable qualitative correlation between the amount of charge transferred and the electronegativity of the TM adatom in question, relatively to Ti and O, which can be found in Ref. [58]. For example, the TMs of group 3 (Sc, Y, and La) have electronegativities considerably lower than that of Ti, and they are the ones which transfer electron density to the Ti_2C surface. Around the center of the periodic table, the TM electronegativity reaches its maximum, which can be a reason for these metals to draw the most charge from the Ti_2C surface. Out of all metals with negative charge transfer when deposited on Ti_2C , Ti is the one that receives the least amount of charge, likely because it is the same metal of which the MXene is made. Nevertheless, some charge transference takes place because the deposited Ti atom is threefold coordinated to other Ti atoms only, while the Ti atoms of Ti_2C are bonded to both C and other Ti. On Ti_2CO_2 , one can almost observe a similar trend, with the amount of charge transferred decreasing more slowly towards the end of each TM series, and finally increasing again near the end. The elements of the last group display lower charge transfers

TABLE III. Calculated diffusion barriers, in eV, of transition metal atoms on the surface of Ti_2C . To facilitate the analysis, the table is color coded from green to red, denoting lower- and higher-energy barriers, respectively.

Sc	Ti	V	Cr	Mn	Fe	Co	Ni	Cu	Zn
0.02	0.10	0.09	0.12	0.19	0.18	0.16	0.14	0.11	0.12
Y	Zr	Nb	Mo	Tc	Ru	Rh	Pd	Ag	Cd
0.03	0.08	0.05	0.14	0.23	0.23	0.20	0.15	0.05	0.08
La/Lu	Hf	Ta	W	Re	Os	Ir	Pt	Au	Hg
0.02	0.07	0.02	0.14	0.19	0.21	0.25	0.24	0.13	0.10

again, an effect related to their very weak interaction with the surface, as seen by their near-zero adsorption energies and long surface-adatom distances.

On both MXenes, the charge-transfer values of first-row TMs are in the same range as the ones reported in the literature [40,41] and follow a similar trend along the period of the periodic table. Indeed, on Ti_2C , both our plot and the one in Ref. [40] display a parabola-like shape. Sc is the only first-row TM which transfers electron density to the surface, of $\sim 0.25 e$. All other metals receive electronic density from the MXene, with the highest absolute value (Fe in our work, Co in Ref. [40]) at nearly $1 e$. The last transition metal, Zn, receives around $0.5 e$ from the surface, as seen in both our plot and that of Ref. [40]. Bader charge transfers on Ti_2CO_2 display the same trends in our work and in Ref. [41] too. All charge transfers are positive; the highest transfer, of almost $2 e$, occurs for Sc, and the lowest one for Zn, with negligible charge transfer, on the opposite end of the first row of TMs. The amount of charge transferred generally decreases along the period, with local maxima occurring for Mn ($\approx 1.4e$) and Cu ($\approx 0.8e$), which also match in our work and in Ref. [41].

There is no direct correlation between the adsorption sites and the adsorption energies or charge transfers, although the adsorption site might be expected to have a direct influence on factors such as charge transfer, due to the number of adjacent atoms and respective adatom-surface distance. There is, however, good correlation between the charge transfer of transition metal atoms on Ti_2C and their Wigner-Seitz radius [38], especially evident for TMs of the second and third rows. This consists of a higher charge transfer being associated with a smaller Wigner-Seitz radius (as seen in Fig. S2 in the Supplemental Material); in other words, atoms that adsorb closer to the surface remove more electrons from it. There is also no direct correlation between the adsorption energy and the charge transfer on Ti_2C . However, on Ti_2CO_2 , less negative adsorption energies (associated to weaker adsorptions) are clearly accompanied by lower charge transfers, showing a very good correlation between the two ($R^2 = 0.87$) (see Fig. S3 of the Supplemental Material).

The diffusion barrier of an adatom corresponds to the energy barrier that must be surpassed for the adatom to travel to the nearest equivalent adsorption site. Using the climbing-image nudged elastic band [59,60] method, we calculated the diffusion-energy barriers for the TM adatoms studied in this work, on the Ti_2C and the Ti_2CO_2 MXene surfaces.

Table III contains the resulting values for Ti_2C . These are all below $0.3 eV$, and the lowest values occur for

TABLE IV. Calculated diffusion barriers, in eV, of transition metal atoms on the surface of Ti_2CO_2 . To facilitate the analysis, the table is color coded from green to red, denoting lower- and higher-energy barriers, respectively.

Sc	Ti	V	Cr	Mn	Fe	Co	Ni	Cu	Zn
1.26	1.40	1.18	0.38	0.52	0.79	0.69	0.72	0.23	0.04
Y	Zr	Nb	Mo	Tc	Ru	Rh	Pd	Ag	Cd
0.93	0.99	1.15	1.46	0.64	0.66	0.40	0.15	0.03	0.04
Lu	Hf	Ta	W	Re	Os	Ir	Pt	Au	Hg
1.13	1.61	1.94	1.32	1.40	1.14	0.88	0.34	0.17	0.02

metals that adsorb on a bridge site. The early and late TM elements require the least energy to travel along the Ti_2C surface. Both these groups of elements adsorb more weakly than the intermediate ones, suggesting that stronger adsorption leads to higher diffusion energy barriers. This is an expected result, since weaker adsorption is related to weaker adsorbent-adsorbate chemical bonds, and naturally leads to more freedom for the adsorbate to move. Overall, these are very low-energy barriers that hint at very flat potential-energy landscapes felt by TM adatoms on Ti_2C . In the literature, information regarding TM adatom diffusion energy on the Ti_2C MXene is only available for Zn, which was estimated at $0.09 eV$ [40], comparable to the $0.12 eV$ obtained here.

The magnitude of TM adatom diffusion-energy barriers along the Ti_2CO_2 MXene surface is significantly different than on Ti_2C , as shown in Table IV. The general trend is for these barriers to decrease along each row, so that metals from group 12 of the periodic table have some of the weakest diffusion barriers. Comparison between the TM diffusion barriers on Ti_2CO_2 with their adsorption energies on the same surface (see Fig. 3) leads us to the same conclusion as on Ti_2C —that lower adatom diffusion barriers are associated with weaker adsorption. Unlike the very low diffusion barriers calculated for Ti_2C , which barely reached $0.2 eV$, those on Ti_2CO_2 are much higher, up to nearly $2 eV$, i.e., TM adatom motion along the Ti_2C MXene surface is kinetically much easier than on Ti_2CO_2 . Since the adatom-Ti distances are similar when the metal atom is adsorbed on Ti_2C and on Ti_2CO_2 , and most adatoms sit on a hollow-carbon site when bound to Ti_2CO_2 , in a sense the oxygen atoms surrounding the metal adatom form a barrier around it, hampering its diffusion. The first-row TM adatom diffusion barriers on Ti_2CO_2 calculated here are systematically lower than the ones obtained in Ref. [41], with differences of up to $0.29 eV$ for Sc. These differences are therefore most likely due to the different-sized supercells used in Ref. [41] and our work. Indeed, the supercell used to model the Ti_2CO_2 MXene in Ref. [41] ensures a distance of about 9 \AA between the TM adatom and its periodic copies, while ours provides a distance of 12 \AA . This implies that in our model, TM adatoms feel less lateral repulsion from their replicas and, consequently, diffuse more easily. This is further supported by the fact that the largest differences between our diffusion barriers and those shown in Ref. [41] occur for the chemical elements with the largest Wigner-Seitz radii.

IV. CONCLUSIONS

In the present work, the adsorption behavior of transition metal atoms on the surfaces of the Ti_2C and Ti_2CO_2 MXenes was investigated.

The presence of oxygen atoms on Ti_2CO_2 causes the majority of the transition metal atoms to adsorb on a hollow-carbon site, whereas on Ti_2C , we found a behavioral pattern for the preferred adsorption site that depends on the number of electrons present in the d -valence subshell of each TM atom. Nevertheless, the distance between the TM adatom and the nearest surface Ti layer is almost the same on both surfaces.

The calculated adsorption energy values are all negative, indicating exothermic adsorption. Their absolute values are quite high for both Ti_2C and Ti_2CO_2 , implying strong interaction between the transition metal atoms and the surface of these MXenes, hinting that the $\text{TM@Ti}_2\text{C}$ and $\text{TM@Ti}_2\text{O}_2$ systems should be stable. The E_{ads} values are of the same order of magnitude on both surfaces, meaning the oxygen surface termination does not significantly affect the adatom behavior in terms of adsorption strength.

When it comes to charge transfer, the presence of an oxygen layer makes a considerable difference, due to the electronegativity of oxygen. On Ti_2CO_2 , all charge-transfer values are positive, meaning electrons were transferred from the adatom to the MXene surface, whereas on Ti_2C , the only TM atoms for which this was the case were Sc, Y, La, and Lu.

All the other TM atoms on Ti_2C become negatively charged after adsorption. On the oxygen-covered MXene, stronger adsorption energies were accompanied by higher charge transfers.

Finally, we calculated the energy barriers for TM adatom diffusion on Ti_2C and Ti_2CO_2 . On the one hand, the values found for Ti_2C are very small, barely reaching 0.2 eV, meaning that the adatoms are subjected to very low “friction” from the surface and can move rather freely along it. On the other hand, on Ti_2CO_2 , many diffusion-energy barriers were predicted to be above 1 eV, which suggests that the oxygen termination layer of the MXene forms a sort of barrier around the adatom, obstructing its diffusion. On both surfaces, the highest diffusion barriers were found to correspond to the TM elements which adsorb most strongly.

ACKNOWLEDGMENTS

This work was developed within the scope of the project CICECO-Aveiro Institute of Materials, Grants No. UIDB/50011/2020, No. UIDP/50011/2020, and No. LA/P/0006/2020, financed by national funds through the FCT/MEC (PIDDAC). We are also thankful to Fundação para a Ciência e a Tecnologia (FCT IP) for the computational resources granted in the framework of Project Ref. No. 2021.09799.CPCA by the FCT/CPCA/2021/01 Call for Advanced Computing Projects.

-
- [1] K. S. Novoselov, A. K. Geim, S. v. Morozov, D. Jiang, Y. Zhang, S. v. Dubonos, I. V. Grigorieva, and A. A. Firsov, Electric field effect in atomically thin carbon films, *Science* **306**, 666 (2004).
- [2] M. Naguib, M. Kurtoglu, V. Presser, J. Lu, J. Niu, M. Heon, L. Hultman, Y. Gogotsi, and M. W. Barsoum, Two-dimensional nanocrystals produced by exfoliation of Ti_3AlC_2 , *Adv. Mater.* **23**, 4248 (2011).
- [3] Y. Gogotsi and B. Anasori, The rise of MXenes, *ACS Nano* **13**, 8491 (2019).
- [4] R. M. Ronchi, J. T. Arantes, and S. F. Santos, Synthesis, structure, properties and applications of MXenes: Current status and perspectives, *Ceram. Int.* **45**, 18167 (2019).
- [5] D. Magne, V. Mauchamp, S. C el erier, P. Chartier, and T. Cabioch, Spectroscopic evidence in the visible-ultraviolet energy range of surface functionalization sites in the multilayer Ti_3C_2 MXene, *Phys. Rev. B* **91**, 201409(R) (2015).
- [6] A. VahidMohammadi, J. Rosen, and Y. Gogotsi, The world of two-dimensional carbides and nitrides (MXenes), *Science* **372**, eabf1581 (2021).
- [7] I. Persson, A. el Ghazaly, Q. Tao, J. Halim, S. Kota, V. Darakchieva, J. Palisaitis, M. W. Barsoum, J. Rosen, and P. O.  . Persson, Tailoring structure, composition, and energy storage properties of MXenes from selective etching of in-plane, chemically ordered MAX phases, *Small* **14**, 1703676 (2018).
- [8] A. Champagne and J.-C. Charlier, Physical properties of 2D MXenes: From a theoretical perspective, *J. Phys. Mater.* **3**, 032006 (2021).
- [9] G. R. Berdiyrov, Optical properties of functionalized $\text{Ti}_3\text{C}_2\text{T}_2$ ($T = \text{F, O, OH}$) MXene: First-principles calculations, *AIP Adv.* **6**, 055105 (2016).
- [10] M. Mozafari and M. Soroush, Surface functionalization of MXenes, *Mater. Adv.* **2**, 7277 (2021).
- [11] J. Bj ork and J. Rosen, Functionalizing MXenes by tailoring surface terminations in different chemical environments, *Chem. Mater.* **33**, 9108 (2021).
- [12] N. Zhang, Y. Hong, S. Yazdanparast, and M. Asle Zaeem, Superior structural, elastic and electronic properties of 2D titanium nitride MXenes over carbide MXenes: A comprehensive first principles study, *2D Mater.* **5**, 045004 (2018).
- [13] X.-H. Zha, K. Luo, Q. Li, Q. Huang, J. He, X. Wen, and S. Du, Role of the surface effect on the structural, electronic and mechanical properties of the carbide MXenes, *EPL* **111**, 26007 (2015).
- [14] J. D. Gouveia, F. Vi nes, F. Illas, and J. R. B. Gomes, MXenes atomic layer stacking phase transitions and their chemical activity consequences, *Phys. Rev. Mater.* **4**, 054003 (2020).
- [15] J. Chen, Q. Huang, H. Huang, L. Mao, M. Liu, X. Zhang, and Y. Wei, Recent progress and advances in the environmental applications of MXene related materials, *Nanoscale* **12**, 3574 (2020).
- [16] B. Anasori, M. R. Lukatskaya, and Y. Gogotsi, 2D metal carbides and nitrides (MXenes) for energy storage, *Nat. Rev. Mater.* **2**, 16098 (2017).
- [17] X. Tang, X. Guo, W. Wu, and G. Wang, 2D metal carbides and nitrides (MXenes) as high-performance electrode materials for lithium-based batteries, *Adv. Energy Mater.* **8**, 1801897 (2018).

- [18] Y. Cui, Z. Cao, Y. Zhang, H. Chen, J. Gu, Z. Du, Y. Shi, B. Li, and S. Yang, Single-atom sites on MXenes for energy conversion and storage, *Small Science* **1**, 2100017 (2021).
- [19] J. Pang, R. G. Mendes, A. Bachmatiuk, L. Zhao, H. Q. Ta, T. Gemming, H. Liu, Z. Liu, and M. H. Rummeli, Applications of 2D MXenes in energy conversion and storage systems, *Chem. Soc. Rev.* **48**, 72 (2019).
- [20] Z. Li, H. Zhang, J. Han, Y. Chen, H. Lin, and T. Yang, Surface nanopore engineering of 2D MXenes for targeted and synergistic multitherapies of hepatocellular carcinoma, *Adv. Mater.* **30**, 1706981 (2018).
- [21] A. Sarycheva, A. Polemi, Y. Liu, K. Dandekar, B. Anasori, and Y. Gogotsi, 2D titanium carbide (MXene) for wireless communication, *Sci. Adv.* **4**, eaau0920 (2018).
- [22] Á. Morales-García, F. Calle-Vallejo, and F. Illas, MXenes: New horizons in catalysis, *ACS Catal.* **10**, 13487 (2020).
- [23] L. Zhang, Y. Ren, W. Liu, A. Wang, and T. Zhang, Single-atom catalyst: A rising star for green synthesis of fine chemicals, *Natl. Sci. Rev.* **5**, 653 (2018).
- [24] S. Ali, Z. Xie, and H. Xu, Stability and catalytic performance of single-atom supported on Ti_2CO_2 for low-temperature CO Oxidation: A first-principles study, *ChemPhysChem* **22**, 2352 (2021).
- [25] J. D. Gouveia, Á. Morales-García, F. Viñes, J. R. B. Gomes, and F. Illas, Facile heterogeneously catalyzed nitrogen fixation by MXenes, *ACS Catal.* **10**, 5049 (2020).
- [26] J. D. Gouveia, G. Novell-Leruth, P. M. L. S. Reis, F. Viñes, F. Illas, and J. R. B. Gomes, First-principles calculations on the adsorption behavior of amino acids on a titanium carbide MXene, *ACS Appl. Bio Mater.* **3**, 5913 (2020).
- [27] J. D. Gouveia, G. Novell-Leruth, F. Viñes, F. Illas, and J. R. B. Gomes, The Ti_2CO_2 MXene as a nucleobase 2D sensor: A first-principles study, *Appl. Surf. Sci.* **544**, 148946 (2021).
- [28] K. Shevchuk, A. Sarycheva, and Y. Gogotsi, Evaluation of two-dimensional transition-metal carbides and carbonitrides (MXenes) for SERS substrates, *MRS Bull.* **47**, 545 (2022).
- [29] M. Zubair, M. M. Ul Hassan, M. T. Mehran, M. M. Baig, S. Hussain, and F. Shahzad, 2D MXenes and their heterostructures for HER, OER and overall water splitting: A review, *Int. J. Hydrog. Energy* **47**, 2794 (2022).
- [30] D. Johnson, B. Hunter, J. Christie, C. King, E. Kelley, and A. Djire, Ti_2N nitride MXene evokes the Mars-van Krevelen mechanism to achieve high selectivity for nitrogen reduction reaction, *Sci. Rep.* **12**, 657 (2022).
- [31] D. Zhao, Z. Chen, W. Yang, S. Liu, X. Zhang, Y. Yu, W.-C. Cheong, L. Zheng, F. Ren, G. Ying, X. Cao, D. Wang, Q. Peng, G. Wang, and C. Chen, MXene (Ti_3C_2) vacancy-confined single-atom catalyst for efficient functionalization of CO_2 , *J. Am. Chem. Soc.* **141**, 4086 (2019).
- [32] A. D. Handoko, H. Chen, Y. Lum, Q. Zhang, B. Anasori, and Z. W. Seh, Two-dimensional titanium and molybdenum carbide MXenes as electrocatalysts for CO_2 reduction, *iScience* **23**, 101181 (2020).
- [33] J. D. Gouveia, Á. Morales-García, F. Viñes, F. Illas, and J. R. B. Gomes, MXenes as promising catalysts for water dissociation, *Appl. Catal. B* **260**, 118191 (2020).
- [34] R. Morales-Salvador, J. D. Gouveia, Á. Morales-García, F. Viñes, J. R. B. Gomes, and F. Illas, Carbon capture and usage by MXenes, *ACS Catal.* **11**, 11248 (2021).
- [35] L. M. Azofra, N. Li, D. R. MacFarlane, and C. Sun, Promising prospects for 2D $d^2 - d^4$ M_3C_2 transition metal carbides (MXenes) in N_2 capture and conversion into ammonia, *Energy Environ. Sci.* **9**, 2545 (2016).
- [36] X. Zhang, B. Shao, Z. Sun, Z. Gao, Y. Qin, C. Zhang, F. Cui, and X. Yang, Platinum nanoparticle-deposited $Ti_3C_2T_x$ MXene for hydrogen evolution reaction, *Ind. Eng. Chem. Res.* **59**, 1822 (2020).
- [37] Y.-H. Chen, M.-Y. Qi, Y.-H. Li, Z.-R. Tang, T. Wang, J. Gong, and Y.-J. Xu, Activating two-dimensional $Ti_3C_2T_x$ -MXene with single-atom cobalt for efficient CO_2 photoreduction, *Cell. Rep. Phys. Sci.* **2**, 100371 (2021).
- [38] B. Hammer and J. K. Nørskov, Theoretical surface science and catalysis—calculations and concepts, *Adv. Catal.* **45**, 71 (2000).
- [39] L. Liu and A. Corma, Metal catalysts for heterogeneous catalysis: From single atoms to nanoclusters and nanoparticles, *Chem. Rev.* **118**, 4981 (2018).
- [40] H. Oschinski, Á. Morales-García, and F. Illas, Interaction of first row transition metals with M_2C ($M = Ti, Zr, Hf, V, Nb, Ta, Cr, Mo$, and W) MXenes: A quest for single-atom catalysts, *J. Phys. Chem. C* **125**, 2477 (2021).
- [41] M. Keyhanian, D. Farmanzadeh, Á. Morales-García, and F. Illas, Effect of oxygen termination on the interaction of first row transition metals with M_2C MXenes and the feasibility of single-atom catalysts, *J. Mater. Chem. A* **10**, 8846 (2022).
- [42] See Supplemental Material at <http://link.aps.org/supplemental/10.1103/PhysRevMaterials.6.105801> for supplemental values and correlations established for transition metal atoms in bare and O-terminated titanium carbide MXenes.
- [43] G. Kresse and J. Hafner, Ab initio molecular dynamics for liquid metals, *Phys. Rev. B* **47**, 558 (1993).
- [44] G. Kresse and J. Hafner, Ab initio molecular-dynamics simulation of the liquid-metal–amorphous-semiconductor transition in germanium, *Phys. Rev. B* **49**, 14251 (1994).
- [45] G. Kresse and J. Furthmüller, Efficient iterative schemes for ab initio total-energy calculations using a plane-wave basis set, *Phys. Rev. B* **54**, 11169 (1996).
- [46] G. Kresse and J. Furthmüller, Efficiency of ab-initio total energy calculations for metals and semiconductors using a plane-wave basis set, *Comput. Mater. Sci.* **6**, 15 (1996).
- [47] J. P. Perdew, K. Burke, and M. Ernzerhof, Generalized Gradient Approximation Made Simple, *Phys. Rev. Lett.* **77**, 3865 (1996).
- [48] S. Grimme, J. Antony, S. Ehrlich, and H. Krieg, A consistent and accurate ab initio parametrization of density functional dispersion correction (DFT-D) for the 94 elements H-Pu, *J. Chem. Phys.* **132**, 154104 (2010).
- [49] S. Grimme, S. Ehrlich, and L. Goerigk, Effect of the damping function in dispersion corrected density functional theory, *J. Comput. Chem.* **32**, 1456 (2011).
- [50] Á. Morales-García, A. Fernández-Fernández, F. Viñes, and F. Illas, CO_2 abatement using two-dimensional MXene carbides, *J. Mater. Chem. A* **6**, 3381 (2018).
- [51] I. Persson, J. Halim, H. Lind, T. W. Hansen, J. B. Wagner, L.-Å. Näslund, V. Darakchieva, J. Palisaitis, J. Rosen, and P. O. Å. Persson, 2D transition metal carbides (MXenes) for carbon capture, *Adv. Mater.* **31**, 1805472 (2019).
- [52] P. E. Blöchl, Projector augmented-wave method, *Phys. Rev. B* **50**, 17953 (1994).
- [53] H. J. Monkhorst and J. D. Pack, Special points for Brillouin-zone integrations, *Phys. Rev. B* **13**, 5188 (1976).

- [54] G. Henkelman, A. Arnaldsson, and H. Jónsson, A fast and robust algorithm for Bader decomposition of charge density, *Comput. Mater. Sci.* **36**, 354 (2006).
- [55] T. A. Manz, Introducing DDEC6 atomic population analysis: Part 3. Comprehensive method to compute bond orders, *RSC Adv.* **7**, 45552 (2017).
- [56] J. Engel, S. Francis, and A. Roldan, The influence of support materials on the structural and electronic properties of gold nanoparticles – a DFT study, *Phys. Chem. Chem. Phys.* **21**, 19011 (2019).
- [57] C. Sun and S. C. Smith, Strong interaction between gold and anatase TiO₂ (001) predicted by first principle studies, *J. Phys. Chem. C* **116**, 3524 (2012).
- [58] A. L. Allred, Electronegativity values from thermochemical data, *J. Inorg. Nucl. Chem.* **17**, 215 (1961).
- [59] G. Henkelman, B. P. Uberuaga, and H. Jónsson, A climbing image nudged elastic band method for finding saddle points and minimum energy paths, *J. Chem. Phys.* **113**, 9901 (2000).
- [60] G. Henkelman and H. Jónsson, Improved tangent estimate in the nudged elastic band method for finding minimum energy paths and saddle points, *J. Chem. Phys.* **113**, 9978 (2000).